International Journal of Mechanical, Industrial and Aerospace Sciences
ISSN: 2517-9950
Vol:6, No:4, 2012

Numerical Evaluation of the Aerodynamic Efficiency of the Stevens and Jolly Vertical-Axis Windmill (1895)

M. Raciti Castelli, E. Benini

***Abstract*—**This paper presents a numerical investigation of the unsteady flow around an American 19th century vertical-axis windmill: the Stevens & Jolly rotor, patented on April 16, 1895. The computational approach used is based on solving the complete transient Reynolds-Averaged Navier-Stokes (t-RANS) equations: a full campaign of numerical simulation has been performed using the *k-ω SST* turbulence model. Flow field characteristics have been investigated for several values of tip speed ratio and for a constant unperturbed free-stream wind velocity of 6 m/s, enabling the study of some unsteady flow phenomena in the rotor wake. Finally, the global power generated from the windmill has been determined for each simulated angular velocity, allowing the calculation of the rotor power-curve.

***Keywords*—**CFD, vertical-axis rotor, windmill.

I. Introduction

WIND power has been used as long as humans have put sails into the wind. The history of windmills shows a general evolution from the use of simple and light devices driven by aerodynamic drag forces to heavy and material-intensive drag solutions. For more than two millennia wind-powered machines have ground grain and pumped water. Wind power was in fact widely available and not confined to the banks of fast-flowing streams. Wind-powered pumps drained the polders of the Netherlands and, in arid regions such as the American deserts or the Australian outback, wind pumps provided water for live stock and steam engines.

As reported by White [1], in the American Midwest between 1850 and 1900, a large number of small windmills, perhaps six millions were installed on farms. The primary use was water-pumping and the main applications were stock watering and farm home water needs. Very large windmills, with rotors up to 18 meters in diameter, were used to pump water for the steam railroad trains that provided the primary source of commercial transportation in areas where there were no navigable rivers.

Marco Raciti Castelli is a Research Associate at the Department of Industrial Engineering of the University of Padova, Via Venezia 1, 35131 Padova, Italy (phone: 0039-3207179239; e-mail: marco.raciticastelli@unipd.it).

Ernesto Benini is an Associate Professor at the Department of Industrial Engineering of the University of Padova, Via Venezia 1, 35131 Padova, Italy (e-mail: ernesto.benini@unipd.it).

To appraise the evolution of windmills from their origin up to the present time demands a considerable investigation work and a wide knowledge of ancient and modern wind turbine mechanics and aerodynamics. Nevertheless, the wide potential of recent numerical techniques based on Computational Fluid Dynamics (CFD), allows tracing back the fundamental steps of the evolution of the modern wind turbine concepts. As a matter of fact, the use of CFD for the design and analysis of vertical-axis wind turbines has aroused a large credit, not only in research and academic communities but also in industrial appliances. A first attempt to improve the efficiency of a vertical-axis wind turbine through the application of the emerging CFD capabilities was performed by Vassberg et al. [2] through the simulation of the dynamic motion of a turbine blade spinning about a vertical axis and subjected to a far-field uniform free-stream velocity flow field.

Raciti Castelli et al. [3] performed a numerical analysis validation campaign for a Darrieus micro Vertical-Axis Wind Turbine (VAWT) through a systematic comparison with wind tunnel experimental data. This work proved that it is possible to determine the best near-blade grid element dimension through statistical analysis of some indicators, such as the y^+ parameter, in order to maximize the accuracy of the numerical prediction of rotor performance, while maintaining a reasonable computational effort.

Ferreira et al. [4] [5] presented a systematic CFD analysis of a two-dimensional blade configuration. The effect of dynamic stall in a 2D single-bladed VAWT was investigated, reporting the influence of the turbulence model in the simulation of the vortical structures spread from the blade.

Kumar et al. [6] proposed a low Reynolds number VAWT design and optimization procedure based on both CFD simulations and BE-M calculations.

Raciti Castelli and Benini [7] presented a model for the evaluation of energy performance and aerodynamic forces acting on a helical single-bladed VAWT depending on blade inclination angle: the analysis was based on five machine architectures, which were characterized by an inclination of the blades with respect to the horizontal plane in order to generate a phase shift angle of 0°, 30°, 60°, 90° and 120° between lower and upper blade sections, for a rotor with an aspect ratio of 1.5.

Raciti Castelli and Benini [8] presented two-dimensional, time-accurate, parallel CFD simulations of the flow field around a three-bladed Darrieus rotor, in order to determine the influence of blade thickness on the operation of a straight-bladed Darrieus-type VAWT.

Raciti Castelli and Benini [9] presented a two-dimensional CFD comparison between the energy performance of two small scale VAWTs, characterized by a 0° and a -1° pitch angle between blade chord and spoke axis.

In the present work a numerical investigation of the unsteady flow around the Stevens & Jolly windmill is presented, in order to assess the CFD potential in analyzing the wind machines of the pre-electrical age. A complete campaign of simulation was performed, investigating flow field characteristics for several values of tip speed ratio and for a constant unperturbed free-stream wind velocity of 6 m/s, thus enabling the study of some unsteady flow phenomena in the rotor wake. Finally, the rotor power-curve was determined, thus evaluating the improvements made in more than 100 years technical evolution of wind power.

II. The Case Study

The presented work is based upon the vertical-axis windmill patented on April 16, 1895 by John H. Stevens and John L. Jolly [10], citizens of the United States residing at Marshfield in the county of Webster and State of Missouri. The object of the invention was to improve the construction of that class of windmills presenting horizontal wind wheels spinning around a vertical axis and to provide a simple and inexpensive means for controlling the admission of wind to the rotor by properly directing the flow to the rotor itself.

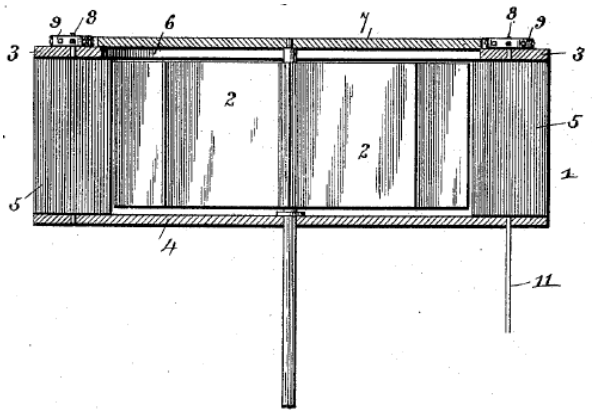

Fig. 1 Vertical view of the Stevens and Jolly windmill (from: [10])

As can be seen from Figs. 1 and 2, showing respectively a vertical and an isometric view of the proposed rotor, the Stevens & Jolly windmill was composed of a circular casing (1), designed to be mounted on a windmill tower and adapted in order to contain a horizontal wind wheel (2), spinning around a central vertical axis. The casing consisted of upper (3) and lower (4) disks and a series of adjustable partitions or shutters (5) arranged at the peripheries of the disks.

The partitions carried sprocket wheels (9) connected by a sprocket chain (10) whereby the shutters were simultaneously operated.

Fig. 3 shows a horizontal section of the rotor. As reported by the inventors, the adjustable partitions could be arranged at any desired angle for admitting air to the wind wheel in the most advantageous manner. The same partitions had also the function of shielding the wind tending to retard the revolution of the windmill or also to stop the rotor by excluding any air passage between them, as evidenced in Fig. 4.

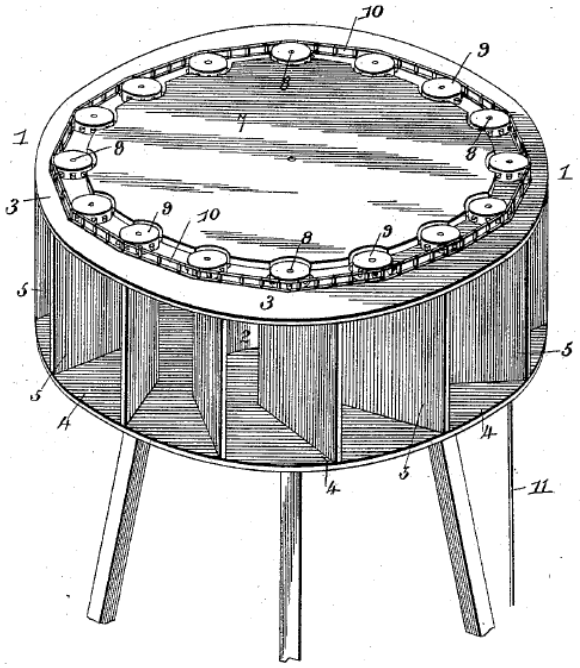

Fig. 2 Isometric view of the Stevens & Jolly windmill (from: [10])

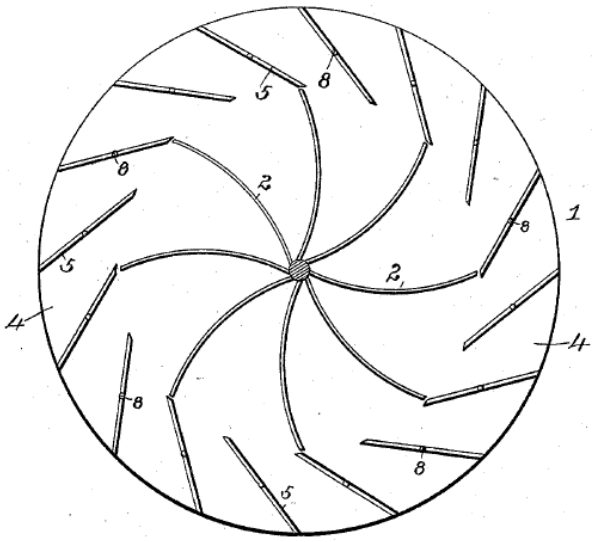

Fig. 3 Horizontal section of the rotor (from: [10])

III. Model Geometry

Fig. 5 shows the numerical model of the tested windmill, corresponding to an arrangement of the adjustable partitions in order to obtain the same configuration shown in Fig. 3. The main geometrical features of the tested rotor are summarized in Table I.

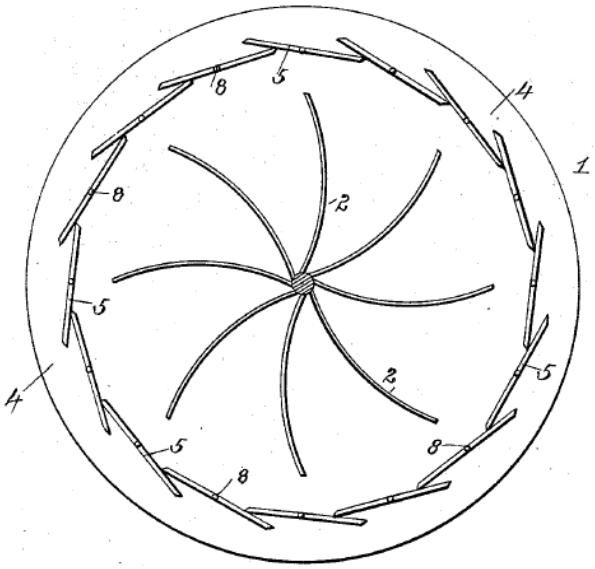

Fig. 4 View of the horizontal section of the rotor completely shielded from external wind by means of the partitions (from: [10])

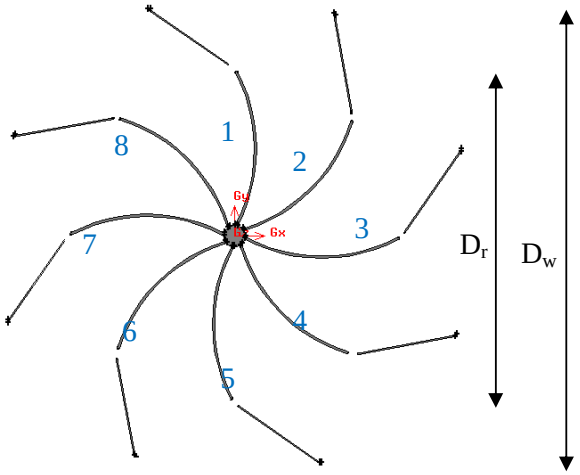

Fig. 5 Numerical model of the tested windmill; rotor blade numbering is also shown (in blue)

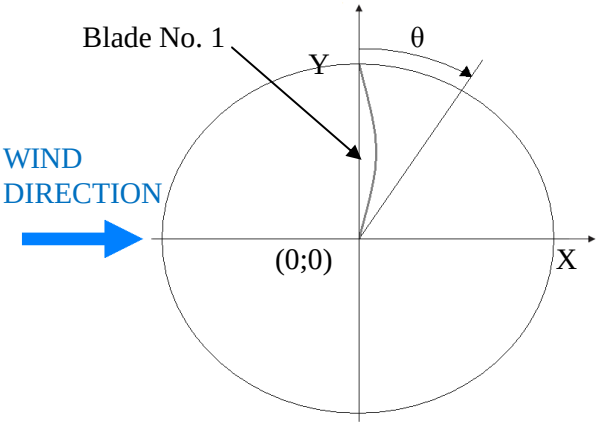

Fig. 6 Azimuthal coordinate of blade No. 1 tip

TABLE I
Main Geometrical Features of the Tested Rotor

Denomination	Value [m]
Windmill external diameter (included the partitions), D_w	5
Rotor diameter, D_r	1.67
Windmill height, H_w	1 (2D simulation)
Rotor height, H_r	1 (2D simulation)

Fig. 6 explains the adopted reference system for the individuation of blade coordinates during rotor revolution: azimuthal position was identified by the angular coordinate of the end tip of blade No. 1, starting between the 2nd and 3rd Cartesian plane octants.

IV. Spatial Domain Discretization

As the aim of the present work was to reproduce the operation of a rotating machine, the use of moving sub-grids was necessary.

In particular, the discretization of the computational domain into macro-areas led to two distinct sub-grids:

- a rectangular outer zone determining the overall calculation domain, with a circular opening centered on the turbine rotational axis, which was identified as *Computational Domain sub-grid*, fixed;
- a circular inner zone, which was identified as *Rotor sub-grid*, rotating with angular velocity ω.

TABLE II
Main Dimensions of the Computational Domain Sub-Grid

Denomination	Value [m]
Computational domain length, L	300
Computational domain width, W	200
Computational domain height, H	1 (2D simulation)

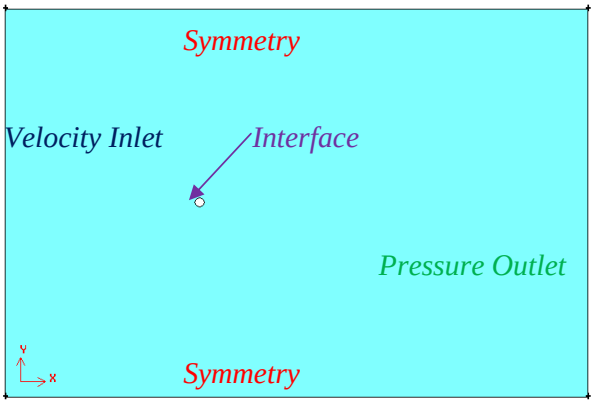

Fig. 7 Boundary conditions of the *Computational Domain sub-grid*

Fig. 7 shows the boundary conditions of the *Computational Domain sub-grid*, while Table II evidences its main dimensions. Inlet and outlet boundary conditions were placed respectively 100 diameters upwind and 200 diameters downwind with respect to the rotor, allowing a full development of the wake, as suggested by the work of Ferreira et al [4]. As can be seen from Fig. 8, an unstructured mesh was chosen, in order to reduce engineering time to prepare the CFD simulations. The boundary of the central hole was set as an *interface*, thus ensuring the continuity of the flow field.

The *Rotor sub-grid* is the fluid area simulating the revolution of the windmill and is therefore characterized by a moving mesh, revolving at the same angular velocity of the rotor. Its location coincides exactly with the hole inside the *Computational Domain sub-grid*. It is good engineering practice to provide that the mesh on both sides of the *interface* (*Rotor sub-grid* and *Computational Domain sub-grid*) has approximately the same characteristic cell size in order to obtain faster convergence [11].

TABLE III
EFFECT OF GRID SPACING ON THE PREDICTED ROTOR TORQUE COEFFICIENT FOR 10 RPM ROTOR ANGULAR VELOCITY

	C_t [-]
Coarser grid (adopted for the numerical simulations of the windmill)	0.064
Finer grid	0.061

TABLE IV
MAIN FEATURES OF THE ADOPTED GRID

Denomination	Value [m]
Grid points uniform spacing on rotor and stator blades [mm]	5
Growth factor from rotor and stator blades [-]	1.2
Grid points maximum spacing on *Rotor sub-grid* area [mm]	50

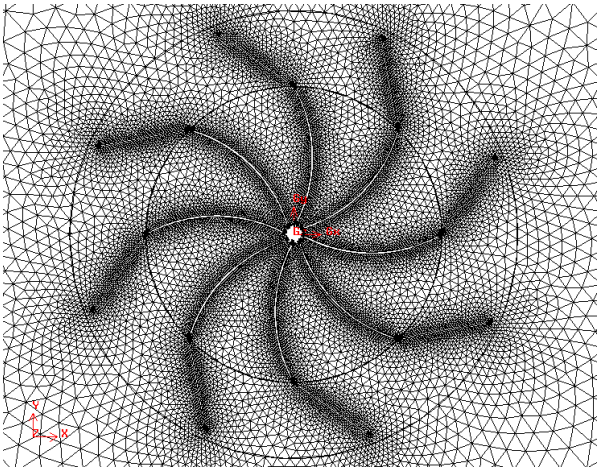

Fig. 8 *Rotor sub-grid* isotropic unstructured mesh

As can be seen from Figs. 8 and 9, an isotropic unstructured mesh was chosen for the *Rotor sub-grid*, in order to guarantee the same accuracy in the prediction of rotor's performance during the rotation – according to the studies of Commings et al. [12] – and also in order to test the prediction capability of a very simple grid. Considering their features of flexibility and adaption capability, unstructured meshes are in fact very easy to obtain, also for complex geometries, and often represent the "first attempt" in order to get a quick response from the CFD in engineering work.

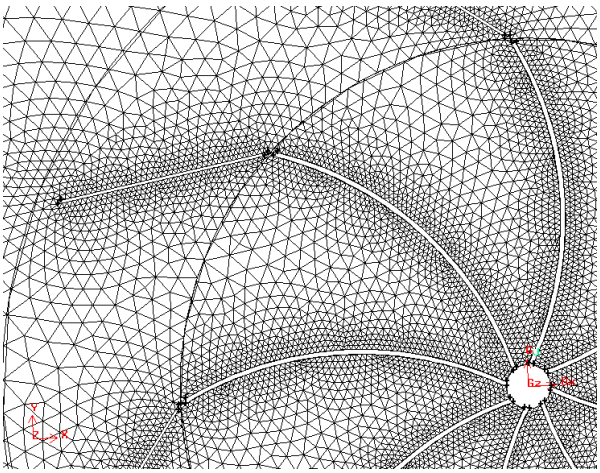

Fig. 9 Detail of near-blade mesh for *Computational Domain sub-grid*

A sensitivity analysis was performed, in order to investigate the influence of the *Rotor sub-grid* spacing, while the *k-ω SST* turbulence model was chosen in accordance to the results of Raciti Castelli et al [3]. A finer grid near the rotor blades was tested and the results obtained using this configuration were compared to those calculated on a coarser grid. As can be seen from Table III, comparisons show a little influence of the grid refinement on the prediction of rotor torque coefficient, defined as:

$$Ct = T / (½ \rho A V_{\infty}^2 R_r) \quad (1)$$

while Table IV shows the main features of the adopted grid.

V. Temporal Discretization and Convergence Criteria

The commercial CFD package ANSYS 12.1®, which implements 2-D Reynolds-averaged Navier-Stokes equations using a finite volume based solver, was adopted for the proposed numerical simulations. The fluid was assumed to be incompressible, being the maximum fluid velocity in the order of 13 m/s. The temporal discretization was achieved by imposing a physical time step equal to the lapse of time the rotor takes to make a 1° rotation. An improved temporal-discretization simulation did not show any significant variation. As a global convergence criterion, each simulation was run until instantaneous torque coefficient values showed a deviation of less than 1% compared with the relative values of the previous period, corresponding to a rotation of 45° due to rotor eight-bladed geometry. Residual convergence criterion for each physical time step was set to 10^{-5}.

The present simulations required about 2 CPU seconds per physical time step. An average value of about 30 sub-iterations was necessary for the solution to converge at each physical time step. Each simulation, performed on a 2.33 GHz clock frequency quad core CPU with Hyper-Threading, required a total CPU time of about 1 day.

VI. Results and Discussion

Fig. 10 represents the evolution of the Stevens & Jolly windmill power coefficient, defined as:

$$C_p = P / (½ \rho A V_{\infty}^3) \quad (2)$$

for an incident wind speed of 6 m/s and as a function of the tip speed ratio, defined as:

$$TSR = \omega R_r / V_{\infty} \quad (3)$$

As can be clearly seen, the range of TSR values is lower than 1, being the driving mechanism of the rotor based upon the aerodynamic drag force. It can also be noticed that the global efficiency of the rotor is quite poor, being the maximum value of the power coefficient of only 2.8% and considering that a modern drag-driven wind turbine typical efficiency can be close to 20% [13]. Nevertheless, it should be remembered that the analyzed rotor geometry was based on an aerodynamic project which dates back over 100 years ago, when the science of aerodynamics was still in its primordial state and in a total absence of numerical techniques which could assist the designers. Besides, a low aerodynamic efficiency is typical of drag-driven wind turbines, while the main argument in favor of these machines is their relatively low construction cost, which makes them less expensive than comparable lift-driven devices, as pointed out by Manwell et al. [14].

Fig. 11 shows the evolution of the torque coefficient as a function of the azimuthal coordinate (defined in Figure 6) for the optimal TSR parameter (0.44): being the Stevens & Jolly windmill composed of 8 blades, a 45° periodicity in rotor dynamic characteristics is registered.

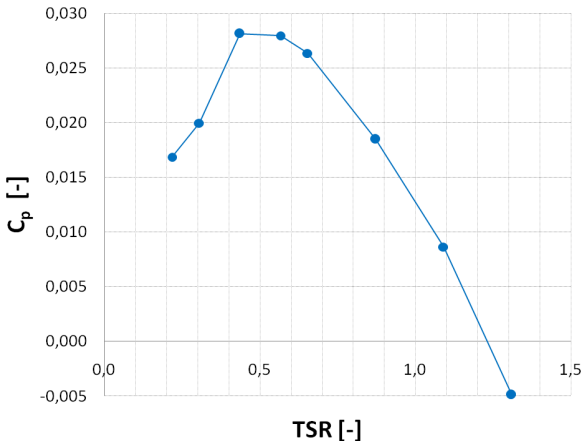

Fig. 10 Evolution of the Stevens & Jolly windmill power coefficient as a function of the tip speed ratio and for an incident wind speed of 6 m/s

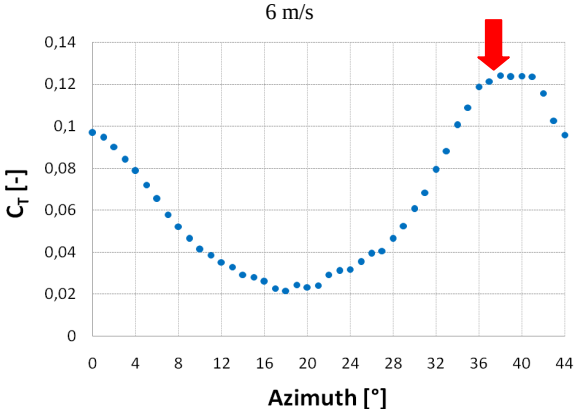

Fig. 11 Evolution of the Stevens & Jolly windmill torque coefficient as a function of the azimuthal coordinate for the optimal TSR parameter (0.44); the red arrow evidences the angular position of maximum torque generation

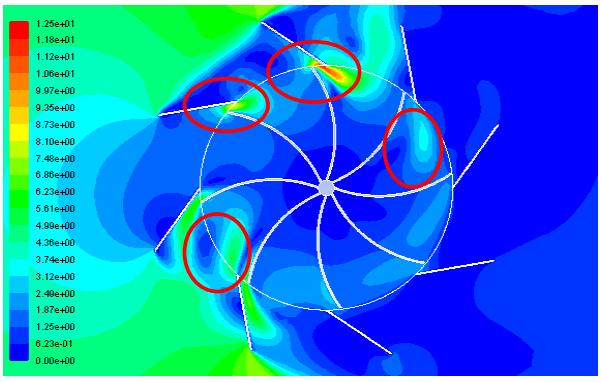

Fig. 12 Contours of absolute velocity [m/s] for maximum rotor torque azimuthal position (θ = 38°). Several recirculation regions are visible (enclosed inside the red circles)

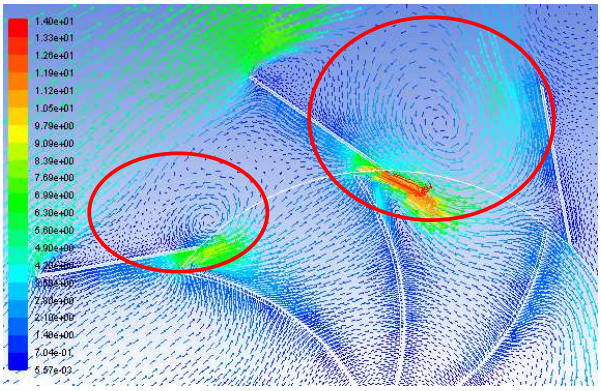

Fig. 13 Absolute velocity vectors [m/s] for maximum rotor torque azimuthal position (θ = 38°). Several recirculation regions are visible (enclosed inside the red circles)

As can be seen from Fig. 12, showing an absolute velocity contour map for the angular position where the maximum rotor torque is registered (evidenced by the red arrow in Fig. 11), the low global efficiency can be explained with the instauration of several recirculation regions inside the rotor, due to a non-optimal interaction between rotor and stator blade aerodynamics. This phenomenon can also be noticed from Fig. 13, showing the absolute velocity vectors for the same angular position: the recirculation zones between stator and rotor blades are clearly visible.

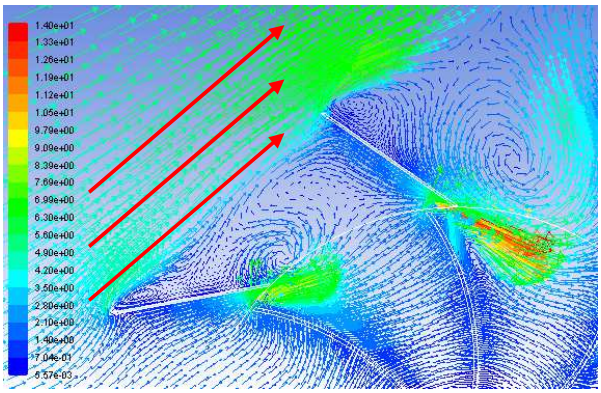

Fig. 14 Absolute velocity vectors [m/s] for maximum rotor torque azimuthal position. Flow separation in correspondence of stator blades (evidenced by the red arrows) can be registered, preventing the flow from entering the rotor zone.

From Fig. 14 an inefficient admission of the air into the wind wheel can be registered, due to flow separation in correspondence of stator blades preventing the flow from entering the rotor zone. Nevertheless, this undesired effect could be reduced by adjusting the external shutters, as suggested by the inventors [10]: further numerical work should be done, in order to investigate the effect of stator blades angle on overall rotor performance, by inclining the partitions and thus admitting the air to the wind wheel in the most advantageous manner.

VII. Conclusions and Future Work

A numerical investigation of the unsteady flow around the Stevens & Jolly windmill was presented, in order to assess the CFD potential in analyzing the wind machines of the pre-electrical age. A complete campaign of simulation was performed, investigating flow field characteristics for several values of tip speed ratio and for a constant unperturbed free-stream wind velocity of 6 m/s.

The global efficiency of the analyzed rotor resulted quite poor, being the maximum value of the power coefficient only 2.8%. This can be explained with the instauration of several recirculation regions inside the rotor, due to a non-optimal interaction between rotor and stator blade aerodynamics and with an inefficient admission of the air into the wind wheel due to flow separation in correspondence of stator blades, thus preventing the flow from entering the rotor zone. This undesired effect could be limited by adjusting the external shutters: further work should be done, in order to investigate the effect of stator blades angle on overall rotor performance, by inclining the partitions and thus admitting the air to the wind wheel in the most advantageous manner.

Nomenclature

A [m^2]	rotor swept area
C_p [-]	rotor power coefficient
C_t [-]	rotor torque coefficient
D_r [m]	rotor diameter
D_w [m]	windmill external diameter (included the partitions)
H_r [m]	rotor height
H_w [m]	windmill height
H [m]	computational domain height
L [m]	computational domain length
R_r [m]	rotor radius
TSR [-]	rotor tip speed ratio
V_∞ [m/s]	unperturbed wind velocity
W [m]	computational domain width
θ [°]	rotor azimuthal coordinate
ρ [kg/m^3]	air density (assumed 1.225)
ω [rpm]	rotor angular velocity

References

[1] L. White Jr., *Medieval technology and social change*, Oxford, 1962, p. 87.

[2] J. C. Vassberg, A. K. Gopinath and A. Jameson, "Revisiting the Vertical-Axis Wind-Turbine Design using Advanced Computational Fluid Dynamics", *AIAA Paper 2005-0047*, 43rd AIAA ASM, Reno, NV.

[3] M. Raciti Castelli, G. Ardizzon, L. Battisti, E. Benini, G. Pavesi, "Modeling Strategy and Numerical Validation for a Darrieus Vertical Axis Micro-Wind Turbine", *ASME 2010 International Mechanical Engineering Congress & Exposition*, November 12-18, 2010, Vancouver (British Columbia), IMECE2010-39548.

[4] C. J. Simao Ferreira, H. Bijl, G. van Bussel and G. van Kuik, "Simulating Dynamic Stall in a 2D VAWT: Modeling Strategy, Verification and Validation with Particle Image Velocimetry Data", *The Science of Making Torque from Wind*, Journal of Physics: Conference Series 75, 2007.

[5] C. Simao Ferreira, G. van Kuik, G. van Bussel and F. Scarano, "Visualization by PIV of dynamic stall on a vertical axis wind turbine", *Experiments in Fluids*, Vol. 46, No. 1, pp. 97-108.
[6] V. Kumar, M. Paraschivoiu and I. Paraschivoiu, "Low Reynolds Number Vertical Axis Wind Turbine for Mars", *Wind Engineering*, Vol. 34, No. 4, June 2010.
[7] M. Raciti Castelli, E. Benini, "Effect of Blade Inclination Angle on a Darrieus Wind Turbine", *ASME Turbo Expo 2010 Gas Turbine Technical Conference*, June 14-18, 2010, Glasgow (Scotland), GT2010-23332
[8] M. Raciti Castelli, E. Benini, "Effect of Blade Thickness on Darrieus Vertical-Axis Wind Turbine Performance", *CSSim 2011 - 2nd International Conference on Computer Modelling and Simulation*, 5-7 September 2011, Brno (Czech Republic).
[9] M. Raciti Castelli, E. Benini, Effect of Negative Pitch Angle on Darrieus Vertical-Axis Wind Turbine Performance, World Academy of Science, Engineering and Technology, Issue 59-2011, pp. 3372-3376.
[10] J. H Stevens and J. L. Jolly, "Windmill", *U.S. Patent No. 537,494*, issued on April 16, 1895.
[11] Fluent Inc., *Fluent User's Manual*, pp. 52, 54, 59, 71, 143.
[12] R. M. Cummings, J. R. Forsythe, S. A. Morton and K. D. Squires, "Computational Challenges in High Angle of Attack Flow Prediction", 2003, Progr. Aerosp. Sci. 39(5):369-384.
[13] J. L. Menet, "A double-step Savonius rotor for local production of electricity: a design study", *Renewable Energy*, Volume 29, Issue 11, September 2004, pp. 1843-1862.
[14] J. F. Manwell, J. G. McGowan and A. L. Rogers, *Wind Energy Explained: Theory, Design and Application*, John Wiley and Sons, 2010, p. 146.